

High-Resolution Range Profile Classifiers Require Aspect-Angle Awareness

Edwyn Brient
STIM, Mines Paris, PSL University
ARC, Thales Land and Air Systems
Fontainebleau/Limours, France
edwyn.brient@minesparis.psl.eu

Santiago Velasco-Forero
STIM, Mines Paris, PSL University
Fontainebleau, France
santiago.velasco@minesparis.psl.eu

Rami Kassab
ARC, Thales Land and Air Systems
Limours, France
rami.kassab@thalesgroup.com

Abstract—We revisit High-Resolution Range Profile (HRRP) classification with aspect-angle conditioning. While prior work often assumes that aspect-angle information is incomplete during training or unavailable at inference, we study a setting where angles are available for all training samples and explicitly provided to the classifier. Using three datasets and a broad range of conditioning strategies and model architectures, we show that both single-profile and sequential classifiers benefit consistently from aspect-angle awareness, with an average accuracy gain of about 7% and improvements of up to 10%, depending on the model and dataset. In practice, aspect angles are not directly measured and must be estimated. We show that a causal Kalman filter can estimate them online with a median error of 5°, and that training and inference with estimated angles preserves most of the gains, supporting the proposed approach in realistic conditions.

Index Terms—HRRP, Classification, Aspect Angle, Radar

I. INTRODUCTION

Recent advances in radar resolution have enabled target representations to evolve from isolated point detections to two-dimensional response maps. However, because of the high scan rate and the large surveillance area, processing such high-resolution grids remains computationally demanding. Consequently, long-range radars commonly compress the target response into a one-dimensional High-Resolution Range Profile (HRRP) by projecting the received echoes onto the radar line of sight (LOS). This dimensionality reduction retains the dominant structural characteristics of the target while significantly decreasing data volume, thereby facilitating real-time processing at the expense of fine-scale spatial details.

The interest in HRRP data for radar automatic target recognition (RATR) has grown significantly over the past decade, driven by the need for rapid onboard classification in dynamic environments. Numerous studies have demonstrated the effectiveness of machine learning methods applied to HRRP data for target classification, both using a single profile as input [1]–[4] and using sequences of profiles [5]–[7]. However, the strong sensitivity of HRRP signals to the aspect angle has only recently been explicitly emphasized. Existing works addressing the impact of aspect angle follow diverse paradigms, including data generation and evaluation

metrics [8], [9], domain adaptation [10], [11], and few-shot classification [12].

We study the benefits of aspect-angle awareness for HRRP classification under realistic angle estimates. Previous works generally assume that aspect-angle information is incomplete in training datasets or unavailable during inference. In contrast, we consider a training scenario in which aspect angles are available for all training samples and analyze the impact of explicitly providing this information to the classifier. Using an extensive set of conditioning mechanisms, model architectures, and three datasets, we show that both single-profile classifiers and sequential classifiers that incorporate aspect-angle information outperform their angle-unaware counterparts. However, in real-world scenarios, aspect angles are not directly measured during acquisition and must be estimated. We first demonstrate that a Kalman filter can estimate the aspect angle accurately in real time. Our final experiments involve training models with estimated aspect angles without degrading classification performance, demonstrating the feasibility of our approach. Some of the data and code used in this work are available at <https://github.com/EdwynBrient/HRRPclf-req-angles>. Our contributions can be summarized as follows:

- **Aspect angle awareness for HRRP classification.** Using both two measured HRRP ship datasets and a MSTAR-derived HRRP dataset, we demonstrate that single-data classifiers and sequential classifiers that are aware of the aspect angle outperform those that are not.
- **Aspect-angle estimation.** We show that a causal Kalman filter estimates ship aspect angles online from AIS kinematics with low error.
- **Practical angle-aware classification.** We demonstrate that conditioning on estimated angles achieves strong performance, supporting deployment when angles are not directly measured.

II. HIGH-RESOLUTION RANGE PROFILE BACKGROUND

A. HRRP Data

A radar measures the backscattered returns of its transmitted waveform and, after standard front-end processing [13], organizes them into a polar map of radar cross section (RCS) values $\sigma(r, \theta)$, indexed by range r (distance) and azimuth θ (bearing). A one-dimensional range profile is obtained by

aggregating RCS values over the azimuth span of the detection cone $[\Theta, \Theta + \Delta\Theta]$:

$$\text{HRRP}(r_i) = \sum_{\theta_j \in [\Theta, \Theta + \Delta\Theta]} \sigma(r_i, \theta_j). \quad (1)$$

The range-bin spacing defines the range resolution Δr .

The HRRP shape depends on the acquisition geometry, primarily governed by the *aspect angle* asp and the *depression angle*. The aspect angle is defined as the relative orientation between the target heading hdg and the radar azimuth θ , i.e., $\text{asp} = hdg - \theta$. The depression angle is the elevation of the radar line of sight (LOS) with respect to the horizontal plane.

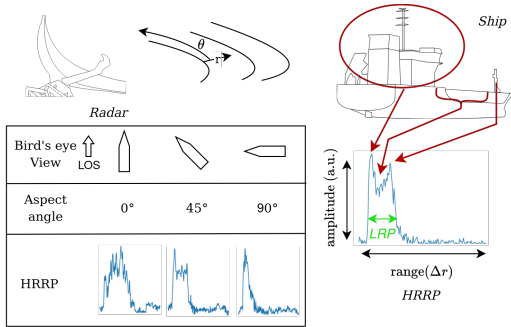


Fig. 1: *HRRP structure and aspect-angle dependence*: an HRRP sums the echoes of dominant scatterers within each range cell; changing asp alters the coarse-scale signature.

Because a 2D scattering distribution is projected onto a 1D profile, HRRPs are not unique: distinct targets can yield similar profiles under certain viewing conditions. In this work, we show that providing aspect-angle information helps reduce this ambiguity and improves classification performance.

B. Aspect Angle and HRRP Geometry

At fine scale, HRRP signatures are not expected to be π -invariant because dominant scatterers and occlusion/shadowing depend on the viewing direction. However, a coarser geometric cue is often close to π -periodic: up to a few strong reflections, the occupied extent along range is mainly driven by the target length projected onto the LOS. This is visible in Fig. 2, where the overall support remains similar for angles separated by π (with noticeable deviations around 135° and 315°).

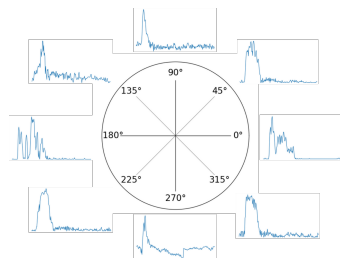


Fig. 2: HRRP of a ship at multiple aspect angles.

The *Length on Range Profile* (LRP) [9] summarizes this support by measuring the range extent of the target response, i.e., an estimate of the LOS-projected length. Fig. 3 illustrates its approximate π -periodicity.

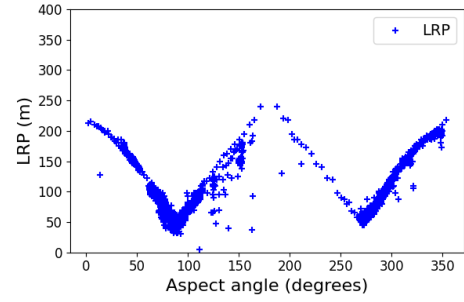


Fig. 3: Length on Range Profile (LRP) [9] across aspect angles.

III. METHODS

A. Models

We evaluate aspect-angle conditioning in two classification settings. In the *single-view* setting, the input is a single HRRP, and the model predicts its class label from that profile alone. In the *multi-view* setting, the input is a temporally ordered sequence of HRRPs acquired along the same target trajectory; the model aggregates per-profile features to produce a single prediction for the sequence.

All models follow a two-stage design: a feature extractor followed by a classifier head. The extractor maps an input HRRP to a compact latent vector, which is then converted into class logits by the head. For single-view experiments, we consider three extractor families: (i) a ResNet-style 1D backbone [14], (ii) a standard convolutional network, and (iii) a multilayer perceptron (MLP). In the multi-view setting, we use the ResNet backbone as the per-profile extractor, as it consistently performed best in our preliminary single-view experiments. To keep the multi-view study focused on temporal aggregation and angle conditioning, we fix this backbone and only vary the sequence model (LSTM, GRU, or Transformer).

All conditioning mechanisms (Sec. III-C) are implemented within the feature extractor. Aspect-angle information is injected at multiple depths: after each residual block (ResNet), after each convolutional block (CNN), and after each hidden layer (MLP). At each injection point, we use a dedicated predictor f_θ that matches the current channel dimension and apply conditioning before the nonlinearity. To account for class imbalance (Fig. 4), we train all models end-to-end with a weighted

cross-entropy loss (inverse class frequencies). In addition to overall accuracy, we report the macro-averaged F1 score, which assigns equal weight to each class. For a given class, precision (P), recall (R), and the F1 score are defined:

$$P = \frac{TP}{TP + FP}, \quad R = \frac{TP}{TP + FN}, \quad F1 = \frac{2PR}{P + R}. \quad (2)$$

where TP, FP, and FN denote true positives, false positives, and false negatives, respectively. The macro-F1 score is computed as the arithmetic mean of the per-class F1 scores giving equal importance to each class regardless of its frequency.

We intentionally rely on standard backbones (ResNet-1D, ConvNet, and MLP) and focus on quantifying the impact

of aspect-angle conditioning and multi-view aggregation on HRRP recognition. Architectural and training hyperparameters are kept fixed across conditioning methods for fair comparison and are provided in the accompanying code repository.

B. Aspect-Angle Estimation

In operational settings, aspect angles are not directly measured and must be estimated from kinematic information. We apply a Kalman filter [15] to denoise position measurements and obtain a smoothed state estimate at each time step, $(x_t, y_t, \dot{x}_t, \dot{y}_t)$, where (x_t, y_t) denotes the target position and (\dot{x}_t, \dot{y}_t) its velocity. The target heading is then computed from the predicted velocity:

$$\widehat{hdg}_t = \text{atan2}(\dot{y}_t, \dot{x}_t), \quad (3)$$

or, when velocities are not part of the state, from successive predicted positions:

$$\widehat{hdg}_t = \text{atan2}(y_t - y_{t-1}, x_t - x_{t-1}). \quad (4)$$

Given the fixed radar position (x_r, y_r) , the line-of-sight (LOS) azimuth from the radar to the target is

$$\widehat{\theta}_t = \text{atan2}(y_t - y_r, x_t - x_r). \quad (5)$$

Following Sec. II-A, we estimate the aspect angle as the difference between heading and LOS azimuth and wrap it to $[0, 2\pi)$:

$$\widehat{\text{asp}}_t = \text{wrap}_{[0, 2\pi)}(\widehat{hdg}_t - \widehat{\theta}_t), \quad (6)$$

where $\text{wrap}_{[0, 2\pi)}(\theta) = \theta - 2\pi \lfloor \frac{\theta}{2\pi} \rfloor$ returns values in $[0, 2\pi)$. The Kalman predictor thus provides both a smoothed kinematic trajectory and the aspect-angle estimates used for conditioning. In our experiments, we split trajectories into segments when the gap between two consecutive measurements exceeds 20 minutes. Kalman parameters are tuned to best match the statistics of our measured trajectories. Kalman estimates are computed online, using only past and current measurements (causal).

C. Conditioning Methods

To incorporate aspect-angle information, we investigate three conditioning strategies commonly used in the literature: concatenation, Feature-wise Linear Modulation (FiLM), and Conditional Batch Normalization (CBN). Let $x \in \mathbb{R}^{N \times C \times L}$ denote an intermediate feature tensor (batch size N , C channels, length L), and let $c \in \mathbb{R}^{N \times D}$ be the associated conditioning vector (D -dimensional angle encoding).

1) *Concatenation*: Concatenation expands c to match the spatial support of x and appends it along the channel dimension. We map c to a scalar token per sample using a linear projection $g_\phi: \mathbb{R}^D \rightarrow \mathbb{R}$, reshape it as $(N, 1, 1)$, and broadcast it along the length axis to obtain $(N, 1, L)$. Concatenating with x yields an augmented feature map of shape $(N, C + 1, L)$.

2) *Feature-wise Linear Modulation (FiLM)*: [16] FiLM conditions x through a per-channel affine modulation. For each sample n , a learnable predictor f_θ (implemented as a linear layer) outputs a scale and shift from c_n :

$$(\gamma(c_n), \beta(c_n)) = f_\theta(c_n), \quad (7)$$

where $\gamma(c_n), \beta(c_n) \in \mathbb{R}^C$. The FiLM output is

$$y_{n,c,l} = \gamma_c(c_n) x_{n,c,l} + \beta_c(c_n), \quad (8)$$

with broadcasting over the length index l .

3) *Conditional Batch Normalization (CBN)*: [17] CBN replaces the standard BatchNorm affine parameters with sample-dependent parameters predicted from c . First, BatchNorm computes channel-wise normalized activations:

$$\widehat{x}_{n,c,l} = \frac{x_{n,c,l} - \mu_c}{\sqrt{\sigma_c^2 + \epsilon}}, \quad (9)$$

where μ_c and σ_c^2 are the batch mean and variance for channel c (computed over indices (n, l)), and $\epsilon > 0$ is a small constant. In CBN, the affine parameters are predicted from the conditioning input:

$$(\gamma(c_n), \beta(c_n)) = f_\theta(c_n), \quad (10)$$

with $\gamma(c_n), \beta(c_n) \in \mathbb{R}^C$. The output is

$$y_{n,c,l} = \gamma_c(c_n) \widehat{x}_{n,c,l} + \beta_c(c_n). \quad (11)$$

FiLM applies a sample-dependent affine transform directly to activations, whereas CBN first normalizes activations using batch statistics and then modulates them via sample-dependent affine parameters.

IV. RESULTS

A. Datasets

We evaluate aspect-angle conditioning on three datasets: an HRRP version of MSTAR and two measured ship HRRP datasets.

a) *MSTAR-HRRP*: We follow [18] to extract HRRPs from the publicly available SAR chips. The resulting dataset contains 10 military vehicle classes with aspect angles spanning $[0^\circ, 360^\circ)$ at a fixed depression angle.

b) *Ship datasets*: Both ship datasets are built from a measured maritime HRRP database, which provides time stamps, AIS-based kinematics, and an AIS-heading-based reference aspect angle (AIS + radar geometry) for each profile. We define two subsets, denoted Ship (A) and Ship (B), to study angle conditioning under different levels of class imbalance and inter-class ambiguity.

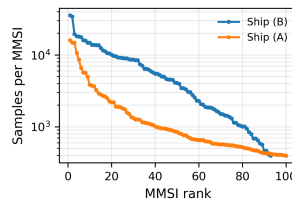


Fig. 4: Sorted MMSI class frequencies for Ship (A) and Ship (B) datasets.

Classes are defined by the ship MMSI (Maritime Mobile Service Identity), i.e., the unique 9-digit identifier assigned to each vessel (100 classes for Ship (A) and 93 for Ship (B)). Fig. 4 indicates that Ship (A) is more class-imbalanced than Ship (B). Moreover, Ship (B) provides more uniform aspect-angle coverage, making it a more reliable setting to evaluate angle-aware learning with fewer angle-class confounds.

Ship (A) includes 100 ships and 185k HRRP profiles. It is intentionally ambiguous: ships exhibit only 24 distinct

TABLE I: One-view classification results with different conditioning methods and architectures (Accuracy | Macro F1 [%]).

Conds	MSTAR			Ship (A)			Ship (B)		
	ResNet	MLP	Conv	ResNet	MLP	Conv	ResNet	MLP	Conv
Uncond	89.46 89.27	62.62 61.89	74.20 73.39	64.29 59.71	27.47 21.60	60.36 53.60	73.62 78.29	37.48 34.05	69.88 72.25
Concat	92.37 91.86	67.50 66.95	83.78 83.05	73.56 68.08	33.24 26.23	69.49 63.30	78.45 83.32	43.28 39.86	68.20 70.71
FiLM	93.60 93.20	69.97 69.69	80.66 79.81	73.28 68.14	32.56 26.18	69.62 63.48	78.61 83.73	42.81 40.04	76.39 80.42
CBN	94.63 94.42	74.20 73.73	80.08 79.46	69.35 63.38	30.34 23.81	64.69 57.51	79.02 84.34	42.81 40.04	76.06 80.19

lengths (mean ≈ 100 m) and five distinct widths, leading to many classes with similar macroscopic geometry. Ship (B) includes 93 ships and about 600k profiles, with more diverse dimensions (12–400 m length) and better coverage of the full 360° aspect-angle range.

B. Aspect-angle estimation quality

In practice, aspect angles are not directly measured and must be estimated from kinematic information. Since we later report results with predicted angles (*Pred aspect*), we first quantify the accuracy of the Kalman-based estimator described in Sec. III-B (Eqs. (3)–(6)).

To this end, we sample 100k contiguous trajectory segments and evaluate the wrapped angular error with respect to the reference aspect angle over increasing context lengths $k \in \{2, \dots, 10\}$. We average errors over k to obtain a segment-level score and also analyze the worst 10% segments to highlight typical failure cases.

Fig. 5 shows that most segments achieve errors below 6° , while the worst 10% concentrate around 20° . Errors decrease with context length, especially for the worst segments. Overall, this accuracy appears sufficient for the following experiments.

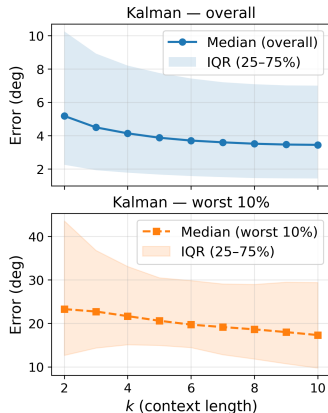


Fig. 5: Kalman-based aspect-angle estimation error over 100k segments (all segments and worst 10%).

C. Experimental setup

To reduce overfitting to exact aspect-angle values, we add Gaussian noise to the conditioning angle ($\sigma=2^\circ$); no jitter is used at validation/test time.

1) *One-view classification*: For one-view classification, we split each dataset into training, validation, and test sets with a 70%/15%/15% ratio using a label-stratified split. We train our three architectures with each conditioning method and compare against an unconditioned baseline.

2) *Multi-view classification*: For multi-view classification, the split requires additional care because adjacent aspect angles tend to cluster within the same time windows. A naive chronological split can therefore induce a shift in aspect-angle

distributions across train/validation/test sets, which hinders generalization.

We sort each ship’s profiles by acquisition time, split them into train/val/test (70/15/15), and build sequences by grouping profiles from the same ship within the same split. A strictly contiguous time split would strongly skew aspect-angle coverage. Our split instead prevents cross-set overlap while keeping angle distributions more comparable, at the cost of less realistic (non-contiguous) sequences since angles along real trajectories are typically more correlated. We only evaluate multi-view models on ships: although MSTAR provides multi-aspect measurements, it does not form operational trajectories, so sequences would be artificial and not meaningful for view aggregation.

D. Results

1) *One-view classification*: Table I reports one-view results. Across datasets and architectures, injecting aspect-angle information improves both accuracy and macro-F1 compared to unconditioned baselines, confirming the benefit of angle awareness for HRRP classification. ResNet consistently achieves the strongest overall performance, motivating its use as backbone in multi-view experiments. FiLM and CBN yield comparable results in most settings; we therefore select CBN in the sequential study.

Table II evaluates conditioning with the estimated aspect angle on the ResNet backbone. Using Kalman-based angles does not noticeably degrade performance compared to using reference angles, and performance remains stable across context lengths k . This suggests that moderate estimation errors have limited impact on recognition, likely due to the inherent noise and intra-class variability of measured HRRPs.

TABLE II: One-view classification with estimated aspect angles on Ship (A)/(B) (Acc./Macro-F1).

Dataset	Conds	k=2	k=5	k=10
		(Acc / Macro F1)	(Acc / Macro F1)	(Acc / Macro F1)
Ship (A)	Uncond	64.29%±0.45%	64.21%±0.61%	64.41%±0.42%
	CBN	67.57%±0.66%	67.95%±0.83%	67.87%±1.03%
Ship (B)	Uncond	73.72%±0.59%	74.01%±0.60%	74.02%±0.82%
	CBN	77.90%±0.21%	77.64%±0.47%	77.78%±0.25%

2) *Multi-view classification*: Table III reports multi-view results on Ship (A) and Ship (B). Without angle input, performance varies widely across sequence models and can remain low on Ship (A), whereas providing aspect angles consistently yields strong accuracy and macro-F1. This gap is smaller on Ship (B), which exhibits more diverse ship dimensions and a more uniform aspect-angle coverage.

TABLE III: Multi-view results on ship datasets (A) and (B) (Accuracy / Macro F1).

Dataset	Conds	LSTM	GRU	Transformer
		(Acc / Macro F1)	(Acc / Macro F1)	(Acc / Macro F1)
Ship (A)	None	43.14%±17.62%	42.26%±6.36%	65.33%±3.50%
		39.63%±19.00%	41.23%±4.65%	66.08%±4.24%
	Real aspect	93.88%±0.16%	94.34%±1.49%	95.54%±4.48%
	Pred aspect	92.20%±0.82%	92.74%±0.85%	96.41%±1.18%
Ship (B)	None	80.43%±1.44%	80.27%±1.43%	79.95%±2.01%
		88.08%±1.70%	88.14%±1.57%	87.50%±2.71%
	Real aspect	87.28%±3.66%	88.31%±1.13%	90.59%±0.89%
		93.00%±2.45%	93.96%±1.37%	96.07%±0.69%
	Pred aspect	88.82%±1.53%	87.79%±2.66%	89.44%±0.99%
		93.89%±0.88%	93.08%±2.06%	95.16%±0.62%

Using Kalman-estimated angles (*Pred aspect*) achieves performance close to using reference angles (*Real aspect*) in the multi-view setting, with differences within run-to-run variability. Finally, using CBN with estimated angles remains stable in our experiments, suggesting robustness to moderate conditioning noise.

V. DISCUSSION

Aspect-angle conditioning improves HRRP classification across datasets, and multi-view aggregation provides additional gains by combining complementary viewpoints. Predicted angles (*Pred aspect*) perform close to reference angles in multi-view experiments, while slightly underperforming in one-view classification, which is expected since estimation noise cannot be averaged out from a single profile.

A key caveat is that angle coverage may differ across vessels: in Ship (A), angle-conditioned models can reach unexpectedly high performance despite strong inter-class ambiguity, suggesting that dataset-specific angle patterns may act as a shortcut cue. In contrast, Ship (B), with more uniform angular coverage, offers a more reliable assessment of the intrinsic benefit of angle awareness.

VI. CONCLUSION

We studied the impact of aspect-angle awareness for HRRP classification in both one-view and multi-view settings, using an HRRP version of MSTAR and two measured maritime datasets. Across architectures and datasets, injecting aspect-angle information consistently improves accuracy and macro-F1, highlighting the central role of acquisition geometry in shaping 1D range signatures. Multi-view aggregation further boosts performance by combining complementary viewpoints along a trajectory.

We also evaluated angle-aware models under imperfect angle inputs using a Kalman-based online estimator. Overall, conditioning on predicted angles yields performance close to using reference angles in the multi-view setting, with a slightly larger gap in one-view classification, supporting the feasibility of angle-conditioned recognition with realistic angle estimates. Finally, our ship experiments underline that angle conditioning can interact with dataset-specific angle coverage; careful control of angle-class correlations is therefore important to obtain unbiased evaluations of multi-view models.

REFERENCES

- [1] J. Wan, B. Chen, B. Xu, H. Liu, and L. Jin, "Convolutional neural networks for radar hrrp target recognition and rejection," *EURASIP J. Adv. Signal Process.*, vol. 2019, pp. 5, 2019.
- [2] M. Bauw, S. Velasco-Forero, J. Angulo, C. Adnet, and O. Airiau, "From unsupervised to semi-supervised anomaly detection methods for hrrp targets," *2020 IEEE Radar Conference (RadarConf20)*, pp. 1–6, 2020.
- [3] L. Sun, J. Liu, Y. Liu, and B. Li, "Hrrp target recognition based on soft-boundary deep svdd with lstm," in *Proc. Int. Conf. Control, Autom. Inf. Sci. (ICCAIS)*, 2021, pp. 1047–1052.
- [4] Y. Diao, S. Liu, X. Gao, A. Liu, and Z. Zhang, "Cnn based on multiscale window self-attention mechanism for radar hrrp target recognition," in *2022 7th International Conference on Signal and Image Processing (ICSIP)*, 2022, pp. 281–285.
- [5] C.-L. Lin, T.-P. Chen, K.-C. Fan, H.-Y. Cheng, and C.-H. Chuang, "Radar high-resolution range profile ship recognition using two-channel convolutional neural networks concatenated with bidirectional long short-term memory," *Remote Sensing*, vol. 13, no. 7, 2021.
- [6] B. Xu, B. Chen, J. Wan, H. Liu, and L. Jin, "Target-aware recurrent attentional network for radar HRRP target recognition," *Signal Processing*, vol. 155, pp. 268–280, 2019.
- [7] X. Wang, P. Wang, Y. Song, Q. Xiang, and J. Li, "Recognition of high-resolution range profile sequence based on tcn with sequence length-adaptive algorithm and elastic net regularization," *Expert Syst. Appl.*, vol. 248, pp. 123417, 2024.
- [8] Y. Song, Q. Zhou, W. Yang, Y. Wang, C. Hu, and X. Hu, "Multi-view hrrp generation with aspect-directed attention gan," *IEEE Journal of Selected Topics in Applied Earth Observations and Remote Sensing*, vol. 15, pp. 7643–7656, 2022.
- [9] E. Brient, S. Velasco-Forero, and R. Kassab, "Mfn decomposition and related metrics for high-resolution range profiles generative models," in *Proc. IEEE Radar Conf. (RadarConf)*. IEEE, 2025, pp. 1–6.
- [10] Y. Wang, Y. Ma, L. Zhang, J. Wang, Y. Zhang, and H. Lv, "Disentanglement model for hrrp target recognition when missing aspects," in *Proc. IEEE Int. Geosci. Remote Sens. Symp. (IGARSS)*, 2023, pp. 5770–5773.
- [11] Y. Wen, L. Shi, X. Yu, Y. Huang, and X. Ding, "Hrrp target recognition with deep transfer learning," *IEEE Access*, vol. 8, pp. 57859–57867, 2020.
- [12] Y. Zhong, W. Lin, Y. Xu, L. Huang, Y. Huang, and X. Ding, "Contrastive learning for radar hrrp recognition with missing aspects," *IEEE Geoscience and Remote Sensing Letters*, vol. 20, pp. 1–5, 2023.
- [13] M. Richards, *Fundamentals Of Radar Signal Processing*, McGraw-Hill Education (India) Pvt Limited, 2005.
- [14] K. He, X. Zhang, S. Ren, and J. Sun, "Deep residual learning for image recognition," in *Proc. IEEE Conf. Comput. Vis. Pattern Recognit. (CVPR)*, 2016, pp. 770–778.
- [15] G. Welch, G. Bishop, and C. Hill, "An introduction to the Kalman filter," pp. 1–16, 1995.
- [16] E. Perez, F. Strub, H. de Vries, V. Dumoulin, and A. C. Courville, "Film: Visual reasoning with a general conditioning layer," in *AAAI*, 2018.
- [17] H. de Vries, F. Strub, J. Mary, H. Larochelle, O. Pietquin, and A. C. Courville, "Modulating early visual processing by language," in *Adv. Neural Inf. Process. Syst.*, I. Guyon, U. V. Luxburg, S. Bengio, H. Wallach, R. Fergus, S. Vishwanathan, and R. Garnett, Eds. 2017, vol. 30, Curran Associates, Inc.
- [18] D. Gross, M. Oppenheimer, B. Kahler, B. Keaffaber, and R. Williams, "Preliminary comparison of high range resolution signatures of moving and stationary ground vehicles," *Proc. SPIE*, vol. 4727, 08 2002.